

ORIGINAL PAPER

Dynamic Interference Prediction and Receive Beamforming for Dense LEO Satellite Networks

Xing Xin¹  | Gaofeng Cui^{1,2}  | Weidong Wang^{1,2}

¹School of Electronic Engineering, Beijing University of Posts and Telecommunications, Beijing, China | ²Key Laboratory of Universal Wireless Communications, Ministry of Education, Beijing, China

Correspondence: Gaofeng Cui (cuiгаofeng@bupt.edu.cn)

Received: 28 September 2024 | **Revised:** 21 January 2025 | **Accepted:** 10 March 2025

Funding: This study was supported by the National Natural Science Foundation of China, grant/award number: 62171052 and the Fundamental Research Funds for the Central Universities, grant/award number: 24820232023YQTD01.

Keywords: DRL | hybrid beamforming | LEO satellite | LSTM

ABSTRACT

Dense low earth orbit (LEO) satellite networks with full frequency reuse can offer seamless global coverage and high spectrum efficiency. However, multiple satellites have overlapping coverage areas, leading to co-channel interference that degrades communication system performance. Moreover, the high dynamic nature of LEO satellites makes the interference varies over time. In this paper, we analyze the receive beamforming to mitigate the complex and time-varying interference in dense LEO satellite networks, and the interference mitigation is formulated as a long-term data rate maximizing problem. To address this problem, a joint intelligent interference prediction and receive beamforming design algorithm is proposed. First, an interference prediction algorithm based on long short-term memory (LSTM) is employed to predict the direction of arrival (DOA) information. Then, a hybrid beamforming algorithm based on deep reinforcement learning (DRL) is proposed to mitigate interference. Simulation results show that the proposed algorithm effectively improves long-term data rate for users and outperforms other benchmark algorithms.

1 | Introduction

Satellite communication offers the advantages of wide coverage and strong resilience to natural disasters, making it an essential component of 6G and a vital extension of terrestrial communication networks [1, 2]. Compared to GEO satellites, LEO satellites provide advantages in terms of lower communication latency and path loss [3]. LEO satellite constellations typically consist of a large number of satellites and exhibit high dynamics, such as Starlink, OneWeb. While sharing spectrum resources among multiple satellites can alleviate the issue of spectrum scarcity, it also introduces the challenge of interference mitigation. Specifically, when different satellites use the same frequency channel in overlapping coverage areas, users in these regions are exposed to complex, time-varying inter-beam and

inter-satellite interference, which can severely degrade communication system performance [4].

LEO satellites are typically multi-beam satellites, which are capable of generating multiple beams simultaneously to serve the unevenly distributed ground users [5]. To mitigate co-channel interference, traditional methods often employ frequency division multiplexing (FDM), such as four-color reuse schemes [6]. However, FDM assigns different frequencies to each beam, which results in lower spectrum utilization efficiency. To improve the spectrum efficiency, full-frequency reuse has been extensively studied in satellite communication systems [7, 8]. Existing methods to mitigate inter-beam interference with full-frequency reuse primarily rely on beam hopping or beamforming techniques. Beam hopping periodically illuminates different

beams in different time slots, and spatial isolation is used to mitigate inter-beam interference [9, 10]. However, beam hopping based on spatial isolation limits the flexibility of beam management and performs poorly in densely populated hotspot areas. Beamforming is also an efficient technique to perform inter-beam interference management [11]. Existing research on satellite communication systems focuses on transmit beamforming for satellite [12–14], but there has been relatively little focus on receive beamforming for mitigating interference. However, multisatellite beam hopping and transmit beamforming schemes require global cooperation among satellites, which involves substantial signaling information exchange. Consequently, receive beamforming design is considered in this paper to mitigate the complex and time-varying interference from satellites. While some studies have explored receiver design to optimize ergodic sum rate, these typically focus on performance within a single time slice [15, 16]. Due to the high dynamics of LEO satellites, the interference at the UT is complex and time-varying. Therefore, it is essential to investigate receive beamforming design to optimize long-term communication in dense LEO satellite networks.

As the strong directionality of satellite channels, receive beamforming design can be designed based on CSI derived from the direction of arrival (DOA) [17]. However, due to the high-speed movement of LEO satellites, the DOA information varies over time, making it challenging to maintain accurate CSI for effective beamforming design. Although DOA information can be obtained through ephemeris data, it is challenging to acquire accurate information regarding interfering satellites. Additionally, ephemeris data are affected by various perturbation factors [18], making it difficult to obtain accurate DOA information. Traditional DOA estimation methods, such as Multiple Signal Classification (MUSIC) and Estimation of Signal Parameters via Rotational Invariance Techniques (ESPRIT), require frequent estimations to obtain DOA information [19, 20]. This process is computationally expensive and difficult to apply directly in dense LEO satellite networks due to the complex and time-varying interference.

In this paper, we study the optimization of the receive beamforming vector to maximize long-term communication performance in dense LEO satellite networks. Unlike existing studies on satellite beam hopping and transmit beamforming that require global information from multiple satellites, this work focuses on optimizing receive beamforming to mitigate interference. Moreover, in contrast to the existing research, which considers the performance of satellite communication systems for a single time snapshot, this paper investigates maximize the long-term communication performance in satellite communication systems. To solve the problem, we model the problem of receive beamforming design for UT to maximize the long-term communication data rate in dense LEO satellite networks. Subsequently, we propose an integrated intelligent DOA prediction and hybrid beamforming design algorithm. The main contributions of this paper are as follows:

- Unlike existing works that focus on receive beamforming design optimization for a single time-slot snapshot, this paper models a framework of maximizing long-term communication data rate with receive beamforming optimization in dense LEO satellite networks. We investigate

interference prediction and receive beamforming design to mitigate complex, time-varying interference.

- To address the influence of high dynamic characteristics of LEO satellites, we propose an intelligent interference prediction method based on long short-term memory (LSTM) for estimating the user's DOA information. The predicted DOA information is used for receive beamforming design.
- For the optimization of the user's long-term communication data rate, we introduce a hybrid beamforming design algorithm based on deep reinforcement learning (DRL). We use the predicted DOA information as input to the Proximal Policy Optimization (PPO) network, which optimizes the analog beamforming, and then optimize the digital beamforming based on the MMSE criterion to maximize the user's long-term communication data rate. Simulation results demonstrate that the proposed scheme outperforms other reference methods.

Notation: We use the following notations in the paper. Matrices and vectors are denoted by bold letters. \hat{a} indicates the estimation value of a . a^T states the transpose of a . a^H states the Hermitian transpose of a . $|a|$ is the magnitude of a . I_N represents the identity matrix of size $N \times N$. $C\mathcal{N}$ is the complex-valued normal distribution.

2 | Related Work

Receive beamforming design has been widely studied in terrestrial systems, where it effectively mitigates interference. However, most of the research has focused on transmit beamforming techniques in satellite communication systems, with relatively little attention to receive beamforming design. To clearly present the state-of-the-art, we will introduce related work in two parts: receive beamforming design for terrestrial systems and receive beamforming design for satellite communication systems.

2.1 | Receive Beamforming Design for Terrestrial Systems

Receive beamforming design has been widely studied in terrestrial systems, where it effectively mitigates and eliminates interference. Son et al. [21] studied interference cancellation in multi-numerology systems through linear receive beamforming design to eliminate inter-numerology interference. Feng et al. [22] analyzed the interchannel interference caused by time-varying channels and proposed an optimization method for receive beamforming to mitigate the interference. Chen et al. [23] investigated the dispersive effect of one-bit quantization on array signals and proposed a subband processing strategy for receive beamforming. Several studies have focused on low-complexity receive beamforming designs for massive MIMO systems. Vasavada et al. [24] proposed a blind iterative projection algorithm for receive beamforming, achieving optimality with lower computational cost compared to singular value decomposition methods. Wang et al. [25] considered hybrid transmit and received beamforming designs for multi-user massive MIMO systems, proposing a low-complexity algorithm based on the equivalent channel to enhance spectral efficiency.

With the rapid development of artificial intelligence, deep learning has been applied to hybrid beamforming design. Liu et al. [26] utilized convolutional neural networks for transmit and receive beamforming design. Zhou et al. [27] studied receive beamforming for high-speed railway scenarios and proposed a deep Q-network algorithm to maximize the average received signal power.

However, the above studies focus on terrestrial systems and do not consider the high dynamics of LEO satellite systems. The complex and time-varying interference that exists in dense LEO satellite networks makes it difficult to apply these approaches directly to LEO systems.

2.2 | Receive Beamforming Design for Satellite Communication Systems

There has been limited research on receive beamforming design specifically for satellite communication systems. Xiang et al. [15] investigated massive MIMO downlink transmission for multiple satellites and proposed a spatial linear receive signal extraction method to handle asynchronous signals from multiple satellites, and a joint design of the precoder and receiver was proposed to maximize the system's ergodic sum rate. Li et al. [16] proposed an optimal linear receiver to improve the SINR, with both satellites and user terminals (UTs) equipped with planar antenna arrays, which demonstrates that single-stream precoding for each user could maximize ergodic rates. Singh et al. [28] studied non-geostationary satellite systems and proposed a linear space-time block-coded signal using a zero-forcing receive beamforming design at the receiver to improve the signal-to-interference-plus-noise ratio (SINR). Besides, many studies have focused on interference mitigation in multi-satellite scenarios through pre-coding. For example, Ding et al. [29] investigated MIMO pre-coding and computation optimization in satellite-terrestrial assisted multilayer computing networks, where MIMO pre-coding was optimized for both UTs and satellites to mitigate interference.

However, the aforementioned multisatellite cooperative schemes require global information sharing among satellites, leading to significant signaling overhead. Additionally, these studies mainly focus on performance at a single snapshot. In contrast, this paper

investigates the optimization of long-term communication performance in dense LEO satellite networks and mitigates complex interference through receive beamforming design.

3 | System Model and Problem Formulation

We consider an LEO satellite communication scenario involving multiple satellites and UTs, as shown in Figure 1. The number of satellites is denoted by S and the number of users by K . The altitude of the satellites is h . Each satellite is equipped with a phased array antenna comprising $N_t = N_{tx} \times N_{ty}$ elements. Similarly, each UT is equipped with a phased array antenna consisting of $N_r = N_{rx} \times N_{ry}$ elements. Each satellite illuminates N_s beams simultaneously to provide service to ground users, each beam serving a single user.

In order to improve the spectral efficiency, the FDM is employed in this paper. Nevertheless, when full frequency reuse is employed, illuminating adjacent beams generates co-channel interference, adversely affecting user data rate. A single satellite can mitigate co-channel interference through spatial isolation [9]. We assume that each satellite illuminates fixed, nonadjacent staring beams on the ground [30]. Despite assuming staring beams, the proposed system model and algorithms are also applicable to beam hopping, as beam hopping can be regarded as a special case of staring beams using time division multiplexing. However, due to the random distribution of users, co-channel interference between different satellites is difficult to avoid. The method proposed in this paper mitigates co-channel interference between different satellites through receive beamforming design.

3.1 | Channel Model

In this paper, we consider a downlink communication scenario involving LEO satellites. The channel model between satellite q and user k can be expressed as follows:

$$\mathbf{H}_{q,k}(t,f) = \sum_{p_h=1}^{P_h} g_{q,k}^{p_h} \exp\left[j2\pi\left(f_{q,k}^{p_h} t - f\tau_{q,k}^{p_h}\right)\right] \mathbf{u}_{q,k,p_h} \mathbf{v}_{q,k,p_h}^H, \quad (1)$$

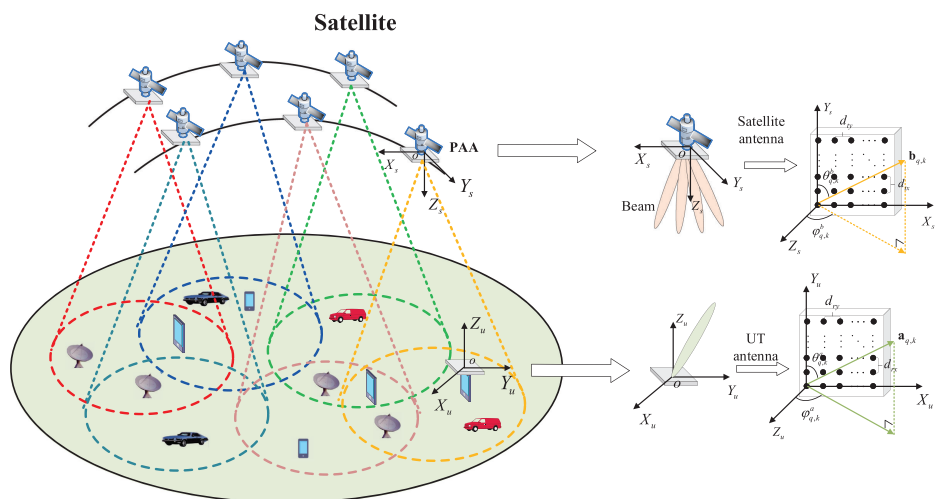


FIGURE 1 | LEO satellite communication scenario.

where $P_h, g_{q,k}^{p_h}, f_{q,k}^{p_h}, \tau_{q,k}^{p_h}, \mathbf{u}_{q,k,p_h} \in \mathbb{C}^{N_r \times 1}$, $\mathbf{v}_{q,k,p_h} \in \mathbb{C}^{N_t \times 1}$ represent the number of multipath, channel gain, Doppler shift, time delay, array response of satellite q , and array response of user k , respectively. The channel gain $g_{q,k}^{p_h}$ includes free-space path loss, shadowing, and atmospheric attenuation [31]. Since the scatterers around a user are located within a few kilometers, while the satellite's orbital altitude is several hundred kilometers, the angles of the different propagation paths for the same user can be considered identical from the satellite's perspective [15]. Thus, $\mathbf{u}_{q,k,p_h} = \mathbf{u}_{q,k}$, $\mathbf{v}_{q,k,p_h} = \mathbf{v}_{q,k}$. The array responses $\mathbf{u}_{q,k}, \mathbf{v}_{q,k}$ can be represented as

$$\mathbf{u}_{q,k} = \left[1, e^{j\frac{2\pi}{\lambda}d_{tx}\beta_{q,k}^u}, \dots, e^{j\frac{2\pi}{\lambda}(N_{rx}-1)d_{tx}\beta_{q,k}^u}, e^{j\frac{2\pi}{\lambda}d_{ty}\alpha_{q,k}^u}, \dots, e^{j\frac{2\pi}{\lambda}(d_{ty}\alpha_{q,k}^u + (N_{rx}-1)d_{tx}\beta_{q,k}^u)}, \dots, e^{j\frac{2\pi}{\lambda}((N_{ry}-1)d_{ry}\alpha_{q,k}^u + (N_{rx}-1)d_{rx}\beta_{q,k}^u)} \right]^T, \quad (2)$$

$$\mathbf{v}_{q,k} = \left[1, e^{j\frac{2\pi}{\lambda}d_{rx}\beta_{q,k}^v}, \dots, e^{j\frac{2\pi}{\lambda}(N_{rx}-1)d_{rx}\beta_{q,k}^v}, e^{j\frac{2\pi}{\lambda}d_{ry}\alpha_{q,k}^v}, \dots, e^{j\frac{2\pi}{\lambda}(d_{ry}\alpha_{q,k}^v + (N_{rx}-1)d_{rx}\beta_{q,k}^v)}, \dots, e^{j\frac{2\pi}{\lambda}((N_{ry}-1)d_{ry}\alpha_{q,k}^v + (N_{rx}-1)d_{rx}\beta_{q,k}^v)} \right]^T, \quad (3)$$

where d_{tx}, d_{ty}, d_{rx} , and d_{ry} denote the spacings between adjacent antenna elements along the x -axis and y -axis for the phased array antennas of the satellite and the user, respectively. $\alpha_{q,k}^u, \beta_{q,k}^u, \alpha_{q,k}^v, \beta_{q,k}^v$ can be denoted as $\alpha_{q,k}^u = \cos(\theta_{q,k}^u), \beta_{q,k}^u = \sin(\theta_{q,k}^u) \sin(\varphi_{q,k}^u), \alpha_{q,k}^v = \cos(\theta_{q,k}^v), \beta_{q,k}^v = \sin(\theta_{q,k}^v) \sin(\varphi_{q,k}^v)$. The terms $\theta_{q,k}^u$ and $\theta_{q,k}^v$ represent the angle of departure (AoD) of the channel, while $\theta_{q,k}^v$ and $\varphi_{q,k}^v$ represent the angle of arrival (AoA) of the channel.

3.2 | Signal Model

A hybrid beamforming structure is shown in Figure 2. Let $\mathbf{W}_k \in \mathbb{C}^{N_r \times 1}$ represent the receive beamforming vector. Due to the high power consumption and computational complexity of digital beamforming with an increasing number of antennas and the lower performance of analog beamforming, a hybrid beamforming architecture is considered at the receiver to balance performance and complexity. The hybrid beamforming is expressed as $\mathbf{W}_k = \mathbf{W}_k^{RF} \mathbf{W}_k^{BB}$, where $\mathbf{W}_k^{RF} \in \mathbb{C}^{N_r \times N_{RF}}$ and $\mathbf{W}_k^{BB} \in \mathbb{C}^{N_{RF} \times 1}$ denote the analog and digital beamforming vector at the receiver, respectively. Additionally, $\|\mathbf{W}_k^{RF}\| = 1$, and \mathbf{W}_k^{RF} can be denoted as

$$\mathbf{W}_k^{RF} = \left[1, e^{j\frac{2\pi}{\lambda}d_{tx}\beta_k^r}, \dots, e^{j\frac{2\pi}{\lambda}(N_{rx}-1)d_{tx}\beta_k^r}, e^{j\frac{2\pi}{\lambda}d_{ty}\alpha_k^r}, \dots, e^{j\frac{2\pi}{\lambda}(d_{ty}\alpha_k^r + (N_{rx}-1)d_{tx}\beta_k^r)}, \dots, e^{j\frac{2\pi}{\lambda}((N_{ry}-1)d_{ry}\alpha_k^r + (N_{rx}-1)d_{rx}\beta_k^r)} \right]^T, \quad (4)$$

where $\alpha_k^r = \cos(\theta_k^r), \beta_k^r = \sin(\theta_k^r) \sin(\varphi_k^r)$. θ_k^r, φ_k^r represent the electrical down-tilt steering and electrical horizontal steering. Let Q' denote the number of interfering satellites, and $Q_J = \{J_1, \dots, J_i, \dots, J_{Q'}\}$ represents the set of interfering

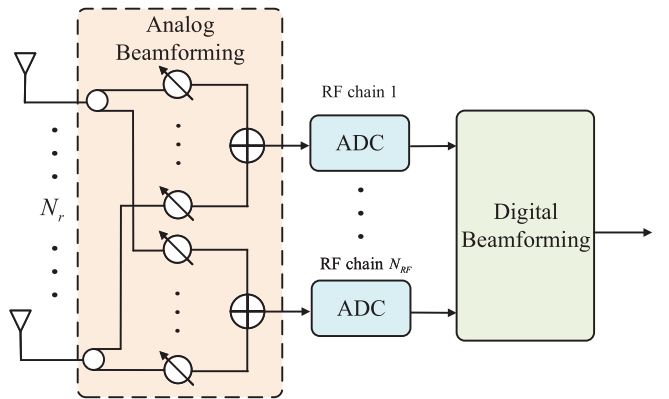


FIGURE 2 | A hybrid beamforming structure.

satellites. Assuming user k is served by satellite q in time slot t , the received signal at user k in time slot t can be expressed as follows:

$$\mathbf{y}_{q,k}(t) = \underbrace{\mathbf{W}_k^H(t)\mathbf{H}_{q,k}(t)\mathbf{F}_{q,k}(t)x_{q,k}(t)}_{\text{desired signal}} + \underbrace{\sum_{j_i \in Q_J} \sum_{n=1}^{N_s} \mathbf{W}_k^H(t)\mathbf{H}_{j_i,k}(t)\mathbf{F}_{j_i,n}(t)x_{j_i,n}(t)}_{\text{interference signals}} + \underbrace{\mathbf{W}_k^H(t)\mathbf{n}}_{\text{noise}}, \quad (5)$$

where $\mathbf{n} \in \mathbb{C}^{N_t \times 1}$ is the additive complex Gaussian noise with $\mathbf{n} \sim \mathcal{CN}(0, \sigma_n^2 I_{N_t})$, and $\mathbf{F}_{q,k} \in \mathbb{C}^{N_t \times 1}$ represent the satellite's transmit beamforming vector for user k . Due to the dense distribution of LEO satellites, users can be served by multiple satellites simultaneously. As a result, user k is susceptible to interference from other satellites. The SINR of user k in time slot t can be expressed as follows:

$$SINR_k(t) = \frac{\left| \mathbf{W}_k^H(t)\mathbf{H}_{q,k}(t)\mathbf{F}_{q,k}(t) \right|^2}{\sum_{j_i \in Q_J} \sum_{n=1}^{N_s} \left| \mathbf{W}_k^H(t)\mathbf{H}_{j_i,k}(t)\mathbf{F}_{j_i,n}(t) \right|^2 + \sigma_k^2}, \quad (6)$$

where $\left| \mathbf{W}_k^H(t)\mathbf{H}_{q,k}(t)\mathbf{F}_{q,k}(t) \right|^2$ represents the desired signal power and σ_k^2 denotes the noise power. $\sum_{j_i \in Q_J} \sum_{n=1}^{N_s} \left| \mathbf{W}_k^H(t)\mathbf{H}_{j_i,k}(t)\mathbf{F}_{j_i,n}(t) \right|^2$ represents the total interference power.

The intrasatellite interbeam interference can be mitigated through spatial isolation. Therefore, this paper primarily focuses on designing the receive beamforming vector to mitigate interference from other satellites. Assuming the channel bandwidth is B_w , the communication data rate of user k in time slot t can be expressed as follows:

$$r_k(t) = B_w \log_2(1 + SINR_k(t)), \quad (7)$$

3.3 | Problem Formulation

The high mobility and density of LEO satellites result in multiple satellites being visible to a user simultaneously. Consequently, users may experience interference from multiple satellites. However, multisatellite MIMO transmit beamforming requires each satellite to obtain global information and requires a large

amount of signaling information exchange. Therefore, this paper considers receive beamforming design, where users periodically update beamforming vectors to mitigate interference from other satellites. The duration of each time slot is represented as Δt , while the beamforming update period and DOA estimation period for user k are denoted by T_k^B and T_k^D , respectively. Unlike most existing works that focus on optimizing a single snapshot, we consider maximizing the long-term communication data rate of each user. The problem can be defined as follows:

$$\mathcal{P}1: \max_{\mathbf{W}_k^{BF}(t), \mathbf{W}_k^{RF}(t)} \sum_{t=1}^{N_T} B_w \log_2(1 + SINR_k(t)), \quad (8a)$$

$$\text{s.t. } |\mathbf{W}_k^{RF}(t)| = 1, t = 1, 2, \dots, N_T, \quad (8b)$$

where N_T denotes the total service time slot. In $\mathcal{P}1$, users experience interference from multiple satellites, with the direction and strength of interference varying across different time slots.

In the dense low Earth orbit (LEO) satellite network environment, which is characterized by high density and rapid variations, timely beamforming must be performed by users to maintain communication performance. The beamforming variable is updated once every time slot, that is, $T_k^B = \Delta t$. However, the frequent updating of beamforming variables requires frequent estimation of DOA information, which is constrained by the limited computational capabilities of terminal devices. To address this limitation, an intelligent interference prediction algorithm has been proposed to reduce computational overhead.

In addition, rapid decisions are required to meet communication rate requirements in rapidly varying environments. Therefore, DRL has been employed in this paper due to its demonstrated ability to enable efficient decision-making after training [27]. The hybrid beamforming algorithm based on DRL has been proposed to leverage the advantages of DRL for adapting to dynamic environments while reducing the computational demands on terminal devices.

4 | Intelligent Hybrid Beamforming Design Based on Interference Prediction

In this section, we propose an intelligent hybrid beamforming design based on interference prediction. First, an LSTM-based

interference prediction algorithm is introduced to obtain the DOA information for different time slots. Then, a hybrid beamforming algorithm based on DRL is employed to further improve the long-term data rate. The network architecture of the proposed algorithm is shown in Figure 3.

4.1 | Intelligent Interference Prediction based on LSTM

To address the challenge of frequent DOA estimation and the associated computational overhead, an interference prediction algorithm based on LSTM is proposed for DOA estimation. The DOA estimation interval is extended to reduce the frequency of estimations. In traditional DOA estimation methods, the DOA information can be accurately estimated in a short estimation period, but it demands large computational resources. On the contrary, in the long estimation period, the computational complexity is reduced by decreasing the number of DOA estimates. However, DOA information changes over time due to the satellite's high dynamics, and the long estimation period cannot be directly applied to DOA information estimation. Thus, the LSTM-based interference prediction algorithm is employed to predict DOA information.

Since long-term DOA information exhibits spatiotemporal characteristics, convolutional LSTM (ConvLSTM) incorporates convolution into the LSTM architecture, allowing the network to effectively capture these spatiotemporal features [32, 33]. The interference prediction network consists of one convolutional layer and two ConvLSTM layers, where the convolutional layer can effectively extract spatial features of input information for subsequent ConvLSTM layer predictions. The ConvLSTM network includes input, forget, and output gates, and the network's processing equations can be expressed as follows:

$$\begin{aligned} \mathbf{i}_t &= \sigma(\mathbf{M}_{xi} * \mathcal{X}_t + \mathbf{M}_{hi} * \mathcal{H}_{t-1} + \mathbf{M}_{ci} * \mathbf{C}_{t-1} + \mathbf{b}_i), \\ \mathbf{f}_t &= \sigma(\mathbf{M}_{xf} * \mathcal{X}_t + \mathbf{M}_{hf} * \mathcal{H}_{t-1} + \mathbf{M}_{cf} * \mathbf{C}_{t-1} + \mathbf{b}_f), \\ \mathbf{C}_t &= \mathbf{f}_t \circ \mathbf{C}_{t-1} + \mathbf{i}_t \circ \tanh(\mathbf{M}_{xc} * \mathcal{X}_t + \mathbf{M}_{hc} * \mathcal{H}_{t-1} + \mathbf{b}_c), \\ \mathbf{o}_t &= \sigma(\mathbf{M}_{xo} * \mathcal{X}_t + \mathbf{M}_{ho} * \mathcal{H}_{t-1} + \mathbf{M}_{co} * \mathbf{C}_t + \mathbf{b}_o), \\ \mathcal{H}_t &= \mathbf{o}_t \circ \tanh(\mathbf{C}_t), \end{aligned} \quad (9)$$

where σ represents the sigmoid function, which can be expressed as $\sigma(x) = \frac{1}{1+e^{-x}}$. The variables \mathbf{i}_t , \mathbf{f}_t , and \mathbf{o}_t denote the input gate, forget gate, and output gate, respectively. \mathcal{H}_t and \mathbf{C}_t represent the hidden state and cell state [34]. The symbols $*$ and \circ denote the

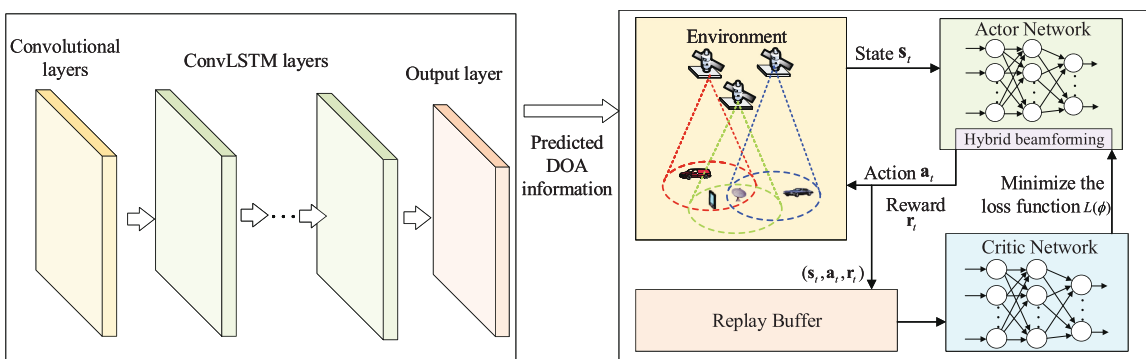


FIGURE 3 | The intelligent interference prediction and hybrid beamforming design.

convolution operation and Hadamard product, respectively. The tanh function, which is used as an activation function, can be expressed as $\tanh(x) = \frac{e^x - e^{-x}}{e^x + e^{-x}}$. The ConvLSTM network structure is shown in Figure 4.

Since DOA information can be estimated using algorithms like MUSIC and ESPRIT, which are prone to estimation errors, we consider the input to the ConvLSTM network as DOA information containing observation noise. The variance of the observation noise is denoted as ζ^2 . We introduce dropout to randomly drop some neurons to avoid overfitting. Besides, batch normalization is added after the convolutional layer and ConvLSTM layers to improve the training speed and stability of the network.

4.2 | Intelligent Hybrid Beamforming Design Algorithm

In this section, hybrid beamforming is designed to improve the long-term data rate for users. As the environment changes in real-time with the movement of satellites, interference mitigation for users must be determined slot by slot. Decisions made in the current time slot will influence choices in the next time slot. Consequently, $\mathcal{P}1$ is formulated as a Markov Decision Process (MDP), which can be defined as follows:

(1) State (**S**): To enhance the long-term communication data rate for users, it is necessary to acquire system information, including the DOA information, $D_t = \{(\theta_{q,k}^b(t), \varphi_{q,k}^b(t)), (\theta_{j_1,k}^b(t), \varphi_{j_1,k}^b(t)), \dots, (\theta_{j_{Q'},k}^b(t), \varphi_{j_{Q'},k}^b(t))\}$, and the signal strength received by the user from the satellites, $Z_t = \{z_{q,k}(t), z_{j_1,k}(t), \dots, z_{j_{Q'},k}(t)\}$. Therefore, the designed state vector can be expressed as follows:

$$\mathbf{s}_t = \{D_t, Z_t\}. \quad (10)$$

(2) Action (**A**): The agent selects an $(\theta_r(t), \varphi_r(t))$ based on Equation (4) to generate $\mathbf{W}_k^{RF}(t)$. To reduce computational complexity, $\mathbf{W}_k^{BB}(t)$ is generated based on the MMSE criterion [35], where $\mathbf{W}_k^{BB}(t) = \left((\mathbf{W}_k^{RF}(t))^H \mathbf{u}_{q,k}(t) \mathbf{u}_{q,k}^H(t) \mathbf{W}_k^{RF}(t) + \sigma_k^2 (\mathbf{W}_k^{RF}(t))^H \mathbf{W}_k^{RF}(t) \right)^{-1} (\mathbf{W}_k^{RF}(t))^H \mathbf{u}_{q,k}(t)$. $\mathbf{u}_{q,k}(t)$ can be calculated using Equation (2) based on the estimated DOA information. The action can be defined as follows:

$$\mathbf{a}_t = \{\theta_r(t), \varphi_r(t)\}. \quad (11)$$

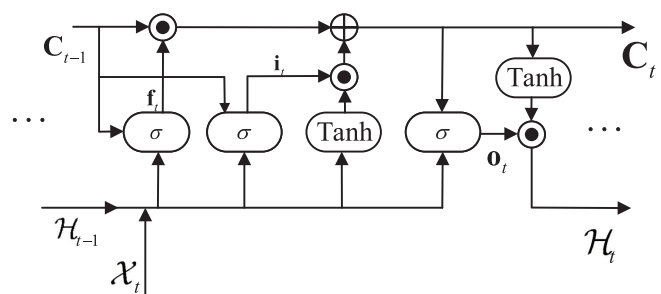


FIGURE 4 | The ConvLSTM network structure.

As the network's optimization goal is to maximize data rate while mitigating interference from other satellites, the $(\theta_r(t), \varphi_r(t))$ are chosen within the 3dB bandwidth range of the desired signal's DOA information to mitigate the interference. Therefore, the range of $(\theta_r(t), \varphi_r(t))$ is $[\theta_{q,k}^b(t) - \Theta_{3dB}, \theta_{q,k}^b(t) + \Theta_{3dB}], [\phi_{q,k}^b(t) - \Phi_{3dB}, \phi_{q,k}^b(t) + \Phi_{3dB}]$, where Θ_{3dB} and Φ_{3dB} represent the 3dB beamwidth of the beam.

(3) Reward (**R**): To maximize the user's communication data rate, the reward value should be defined in terms of the communication data rate. Since the SINR for each time slot can be calculated based on Equation (6), the reward value for each time slot can be represented as

$$r_t = \text{SINR}_k(t). \quad (12)$$

Given the large state and action spaces in this paper, modeling the transition probabilities is challenging. Therefore, a model-free Markov process is adopted, with DRL based on PPO employed for the hybrid beamforming design. The PPO algorithm utilizes an actor-critic framework and is a type of policy gradient algorithm. The policy $\pi_\xi(s_t, a_t)$ represents the probability of taking action a_t in state s_t , and can be expressed as follows:

$$\pi_\xi(s_t, a_t) = P(a_t | s_t), \quad (13)$$

where ξ denotes the parameters of the actor network. The PPO algorithm updates ξ during each iteration to maximize its loss function. The loss function $L^{clip}(\xi)$ can be expressed as follows:

$$L^{clip}(\xi) = \left[\min(\vartheta_t(\xi), \text{clip}\{\vartheta_t(\xi), 1 - \varepsilon, 1 + \varepsilon\}) \hat{A}_t \right]. \quad (14)$$

The term $\text{clip}(\vartheta_t(\xi), 1 - \varepsilon, 1 + \varepsilon)$ is a clipping function designed to limit the rate at which the policy updates. Here, $\vartheta_t(\xi)$ represents the probability ratio between the new policy and the old policy, which can be expressed as follows:

$$\vartheta_t(\xi) = \frac{\pi_\xi(s_t, a_t)}{\pi_{\xi_{\text{old}}}(s_t, a_t)}. \quad (15)$$

In Equation (14), \hat{A}_t denotes the generalized advantage estimation, which can be expressed as follows:

$$\hat{A}_t = R_t - V_\psi(s_t), \quad (16)$$

where $V_\psi(s_t)$ is generated by the critic network and represents the state value function and R_t represents the discounted reward function, which can be expressed as follows:

$$R_t = \sum_{i=t}^{T-1} r_i \gamma^{i-t} + \gamma^{T-t} V_\phi(s(t)). \quad (17)$$

The parameter ϕ is updated by minimizing the critic network's loss function $L(\phi)$, which can be expressed as follows:

$$L(\phi) = \frac{1}{T} \sum_{t=1}^T (V_\phi(s(t)) - R_t)^2 \quad (18)$$

After multiple iterations, the network's reward values and loss values gradually converge, and the optimized policy can maximize the long-term user communication data rate. The intelligent hybrid beamforming design algorithm based on PPO is shown in Algorithm 1.

5 | Simulation Results

In this paper, we consider the dense LEO satellite network involving 6372 satellites at 1200-km altitude, and the carrier frequency is 20 GHz. Each satellite can generate four beams to cover the ground area. We select three users to simulate and validate the proposed algorithm. The minimum elevation angle for each user is set to 55° [36]. The total service time is 200 s, and each time slot is set to 1 s. The intelligent interference prediction based on LSTM employs a prediction network consisting of one convolutional layer, two ConvLSTM layers, and one fully connected layer. In the intelligent hybrid beamforming design algorithm, the PPO network includes two hidden layers and one output layer, with the tanh function used as the activation function. The main system parameters are shown in Table 1.

To evaluate the performance of the proposed intelligent interference prediction algorithm based on LSTM (IP-LSTM), we compare it with the Kalman filter (KF) algorithm [37]. The observation noise variance is set to $\zeta^2 = 0.1$. Since time slot duration Δt is 1 s, we simulate different DOA estimation periods $T_k^D \geq \Delta t$ to verify the algorithm's predictive performance. Figure 5 shows the root mean square error (RMSE) of DOA prediction versus the DOA estimation period. It can be seen that the RMSE of the predicted DOA increases with a longer DOA estimation period. Although the RMSE of the IP-LSTM algorithm also increases with longer DOA estimation periods, the rate of increase remains relatively small compared to the KF algorithm. Therefore, it can be observed that decreasing the DOA estimation period improves prediction accuracy, but it requires more frequent estimations and increases computing resource consumption. Based on this trade-off, a DOA estimation period of 3 s is selected for the subsequent simulations, as the learning rate plays a critical role in the training performance of PPO networks. Therefore, both fixed and dynamic learning rates are analyzed in this paper. The dynamic learning rate varies across episodes, with two specific cases considered as follows:

Algorithm 1 Intelligent Hybrid Beamforming Design Algorithm based on PPO

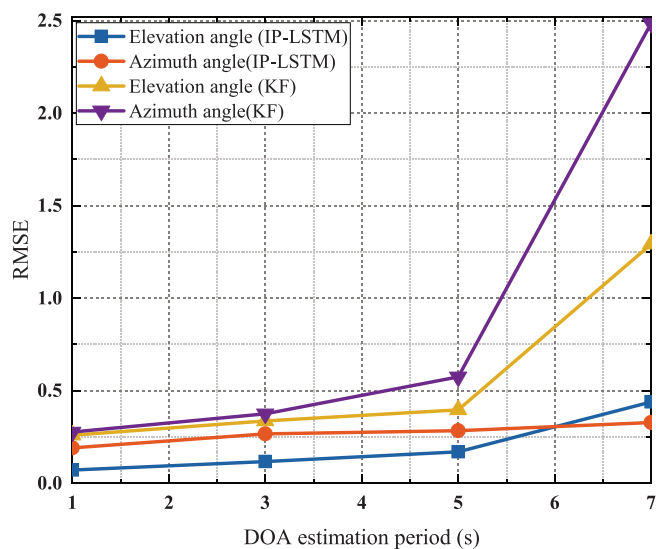
```

Input: The DOA information of users  $\mathcal{D}_t$ ,  $\mathcal{Z}_t$ .
Output: Optimized hybrid beamforming  $\{\mathbf{W}_k^{RF}(t)$ ,  $\mathbf{W}_k^{BB}(t)\}$ .
1: Initialize the replay buffer  $\mathcal{D}$ , the actor network parameter  $\xi_0$ , the critic
   network parameter  $\phi_0$ .
2: for episode  $ep = 1, 2, \dots, N_{Ep}$  do
3:   while the replay buffer is not full do
4:     Initialize the state  $s_0$ ;
5:     for step  $k = 1, 2, \dots, N_t$  do
6:       Choose an action  $a_t$  based on the policy
           $\pi_\vartheta(a, s)$ ;
7:       Based on the current action  $a_t$ , the next state
           $s_{t+1}$  and the current reward  $r(s_t, a_t)$ 
          are given by the environment;
8:       Store  $(s_t, a_t, r(s_t, a_t), s_{t+1})$  into
          the replay buffer  $\mathcal{D}$ ;
9:       Calculate the advantage function  $\hat{A}_t$ ;
10:      end for
11:    end while
12:    for update iteration  $j = 1, 2, \dots, N_m$  do
13:      Randomly sample minibatch of transitions from
          the replay buffer  $\mathcal{D}$ ;
14:      Update the critic network parameter  $\phi$  by
          minimizing the loss function  $L(\phi)$  via (18);
15:      Update the actor network parameter  $\xi$  by
          maximizing the loss function  $L^{clip}(\xi)$  via (14).
16:    end for
17:    Update old actor network with  $\vartheta_{old} = \vartheta$ ;
18:    Clear the replay buffer  $\mathcal{D}$ ;
19:  end for

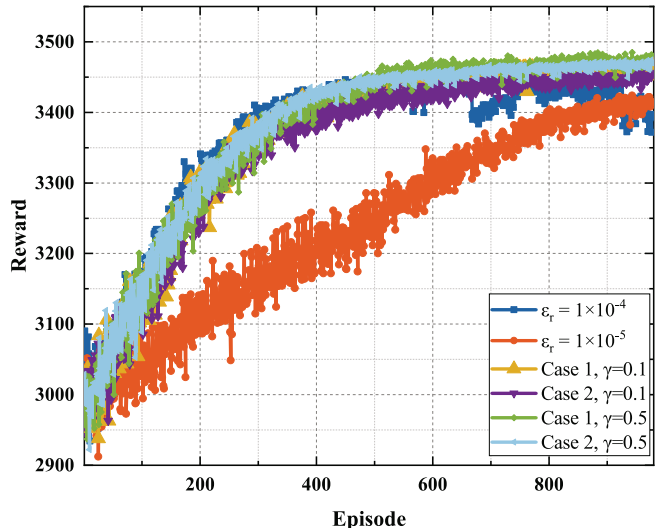
```

TABLE 1 | Simulation parameters.

Parameters	Value
Satellite altitude	1200 km
Carrier frequency	20 GHz
Channel bandwidth	400 MHz
Minimum visibility elevation angle of the UT	55°
Max gain of satellite antenna	38.5 dBi
The number of UT antenna	24 × 24
System temperature	290 K
ConvLSTM parameters	
Filters	128
Kernel size	2 × 2
Training epochs	10,000
PPO parameters	
Number of neurons per layer	128
Discount factor	0.99
Maximum training episodes	20,000
Clip function hyperparameter	0.2
Replay buffer size	4096
Minibatch size	1024
Number of steps per episode	200
Optimization epochs	20

**FIGURE 5** | The RMSE versus the DOA estimation period.

$$\begin{aligned} \text{Case1 : } \epsilon_r &= \begin{cases} \epsilon_i, & ep \leq N_{ep}/2, \\ \epsilon_i \times \gamma, & ep > N_{ep}/2, \end{cases} \\ \text{Case2 : } \epsilon_r &= \begin{cases} \epsilon_i, & ep \leq N_{ep}/4, \\ \epsilon_i \times \gamma, & N_{ep}/4 < ep \leq N_{ep}/2, \\ \epsilon_i \times \gamma^2, & ep > N_{ep}/2, \end{cases} \end{aligned} \quad (19)$$

**FIGURE 6** | Convergence of intelligent hybrid beamforming design algorithm.

where N_{ep} is the maximum number of episodes. ϵ_r denotes the current learning rate, ϵ_i is the initial learning rate, and γ is the control variable. With the initial learning rate set to $\epsilon_i = 1 \times 10^{-4}$, the simulation results are shown in Figure 6.

Figure 6 illustrates the convergence characteristics under different learning rate strategies. With a fixed learning rate, $\epsilon_i = 1 \times 10^{-4}$ converges faster than $\epsilon_i = 1 \times 10^{-5}$ but results in instability in later episodes. In contrast, $\epsilon_i = 1 \times 10^{-5}$ leads to slower but more stable convergence. For dynamic learning rate, the value of γ has a significant impact on performance. A smaller γ slows convergence due to a rapid decrease in the learning rate, which negatively impacts performance in later episodes. Among the tested scenarios, Case 1, with $\gamma = 0.5$ achieves the best balance between reward and stability. Therefore, this dynamic learning rate has been adopted for subsequent simulations.

To verify the effectiveness of the proposed algorithm, we analyzed the performance of existing algorithms and the algorithm proposed in this paper. The reference algorithm and the algorithm proposed in this paper are explained as follows:

- Intelligent interference prediction based on LSTM and beam steering (IPLSTM-BS): The intelligent interference prediction algorithm is used for DOA estimation, and beam steering is performed towards the satellite by users based on the predicted DOA [38].
- IPLSTM and OMP hybrid beamforming (IPLSTM-OMP): The IPLSTM algorithm is used for DOA prediction, and the OMP algorithm [39] is applied for hybrid beamforming.
- IPLSTM and MMSE-based beamforming design (IPLSTM-MMSE): The IPLSTM algorithm is used for DOA prediction, and fully digital MMSE [40] is adopted for beamforming.
- KF and intelligent hybrid beamforming design (KF-IHB): The KF algorithm is used for DOA prediction, while the hybrid beamforming design uses the proposed method in this paper.
- Intelligent interference prediction based on LSTM and intelligent hybrid beamforming (IPLIHB): The intelligent

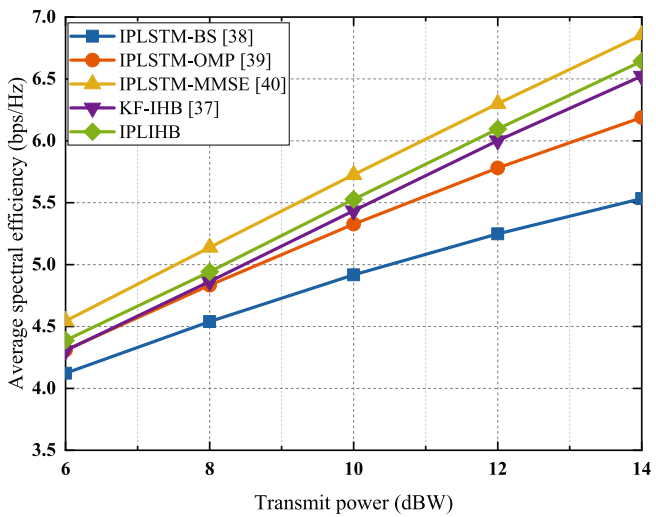


FIGURE 7 | Average spectral efficiency versus the transmit power.

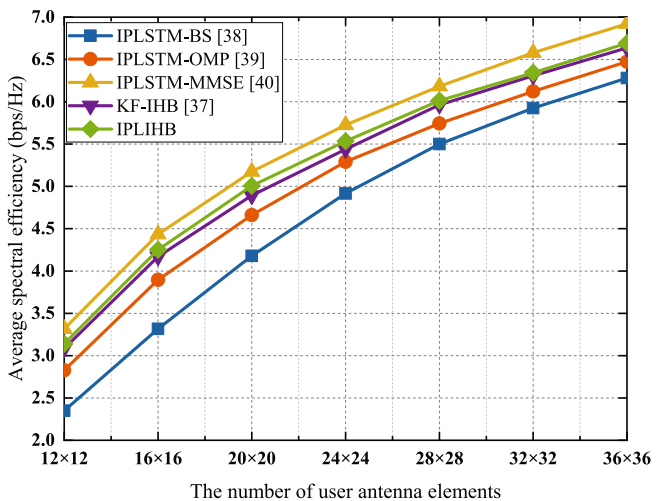


FIGURE 8 | Average spectral efficiency versus the number of user antenna elements.

interference prediction and hybrid beamforming design algorithm proposed in this paper.

The variation in average spectral efficiency with respect to satellite transmit power is shown in Figure 7. As transmit power increases, the average spectral efficiency of users also increases. Algorithms employing hybrid beamforming outperform the utilizing beam steering. The IPLIHB algorithm demonstrates superior performance compared to the other methods, though it is slightly lower than the fully digital beamforming IPLSTM-MMSE. Additionally, since the DOA estimation accuracy of the KF algorithm is lower than that of IP-LSTM, the IPLIHB algorithm outperforms the KF-IHB algorithm.

Besides, we analyzed the computational complexity of the proposed algorithm. The complexity of the proposed LSTM-based DOA prediction algorithm primarily depends on the number of input channels C_i , the number of output channels C_o , and the kernel size N_k . It can be expressed as $\mathcal{O}(4(C_i C_o N_k^2 + C_o^2 N_k^2))$ [41]. In the hybrid beamforming computation, the complexity of the DRL-based beamforming algorithm is influenced by the sizes of the input layer, hidden layers, and output layer. Specifically, the

dimension of the input layer depends on the state space, and the size of the output layer depends on the action space. Let the size of the state space be X_s , the size of the action space be X_a , and the size of the hidden layer be N_h . The complexity of the DRL-based beamforming algorithm is therefore given as $\mathcal{O}(X_s N_h + N_h^2 + N_h X_a)$ [42]. Additionally, the computational complexity of solving the digital part of the hybrid beamforming is $\mathcal{O}(N_{RF}^3)$, where N_{RF} represents the number of RF chains. Thus, the total complexity of the IPLIHB algorithm can be expressed as $\mathcal{O}(4(C_i C_o N_k^2 + C_o^2 N_k^2) + X_s N_h + N_h^2 + N_h X_a + N_{RF}^3)$.

Figure 8 illustrates the performance variation of average spectral efficiency as the number of user antenna elements increases. In Figure 8, it can be observed that the average spectral efficiency improves as the number of antennas increases. Because of the larger number of antennas, the 3dB bandwidth of each antenna is reduced, which lowers the interference experienced by users and consequently enhances performance. Furthermore, the IPLIHB algorithm performs better than other algorithms across different numbers of antennas, remaining slightly lower than the fully digital beamforming method IPLSTM-MMSE. Although the fully digital MMSE scheme achieves superior performance, it requires each antenna element to be equipped with a separate radio frequency (RF) chain and analog-to-digital (ADC) converters. As a result, the fully digital MMSE scheme incurs significant costs and power consumption due to the high number of RF chains [43]. In contrast, the proposed hybrid beamforming scheme uses fewer RF chains, which effectively reduces the complexity and power consumption of the equipment.

6 | Conclusion

This paper investigates interference prediction and hybrid beamforming design in dense LEO satellite networks. In LEO satellite networks, overlapping satellite coverage areas under full-frequency reuse cause complex, time-varying interference, significantly degrading communication performance. To tackle this issue, an intelligent interference prediction algorithm is proposed to estimate DOA information. Subsequently, a PPO-based hybrid beamforming algorithm is introduced to mitigate multi-satellite interference. Simulation results show the effectiveness of the proposed algorithm.

Conflicts of Interest

The authors declare no conflicts of interest.

References

- H. Guo, J. Li, J. Liu, N. Tian, and N. Kato, “A Survey on Space-Air-Ground-Sea Integrated Network Security in 6G,” *IEEE Communications Surveys & Tutorials* 24, no. 1 (2022): 53–87, <https://doi.org/10.1109/COMST.2021.3131332>.
- D. C. Nguyen, M. Ding, P. N. Pathirana, et al., “6G Internet of Things: A Comprehensive Survey,” *IEEE Internet of Things Journal* 9, no. 1 (2022): 359–383, <https://doi.org/10.1109/JIOT.2021.3103320>.
- G. Pan, J. Ye, J. An, and M.-S. Alouini, “Latency Versus Reliability in LEO Mega-Constellations: Terrestrial, Aerial, or Space Relay?,” *IEEE*

- Transactions on Mobile Computing* 22, no. 9 (2023): 5330–5345, <https://doi.org/10.1109/TMC.2022.3168081>.
4. X. Chen and Z. Luo, “Asynchronous Interference Mitigation for LEO Multi-Satellite Cooperative Systems,” *IEEE Transactions on Wireless Communications* 2024 (2024): 1–1, <https://doi.org/10.1109/TWC.2024.3422101>.
 5. H. Xv, Y. Sun, Y. Zhao, M. Peng, and S. Zhang, “Joint Beam Scheduling and Beamforming Design for Cooperative Positioning in Multi-Beam LEO Satellite Networks,” *IEEE Transactions on Vehicular Technology* 73, no. 4 (2024): 5276–5287, <https://doi.org/10.1109/TVT.2023.3332142>.
 6. F. Rinaldi, H.-L. Mttnen, J. Torsner, et al., “Broadcasting Services Over 5G NR Enabled Multi-Beam Non-Terrestrial Networks,” *IEEE Transactions on Broadcasting* 67, no. 1 (2021): 33–45, <https://doi.org/10.1109/TBC.2020.2991312>.
 7. T. Shi, Y. Liu, S. Kang, S. Sun, and R. Liu, “Angle-Based Multicast User Selection and Precoding for Beam-Hopping Satellite Systems,” *IEEE Transactions on Broadcasting* 69, no. 4 (2023): 856–871, <https://doi.org/10.1109/TBC.2023.3294838>.
 8. E. Kim, I. P. Roberts, and J. G. Andrews, “Downlink Analysis and Evaluation of Multi-Beam LEO Satellite Communication in Shadowed Rician Channels,” *IEEE Transactions on Vehicular Technology* 73, no. 2 (2024): 2061–2075, <https://doi.org/10.1109/TVT.2023.3312977>.
 9. Z. Lin, Z. Ni, L. Kuang, C. Jiang, and Z. Huang, “Multi-Satellite Beam Hopping Based on Load Balancing and Interference Avoidance for NGSO Satellite Communication Systems,” *IEEE Transactions on Communications* 71, no. 1 (2023): 282–295, <https://doi.org/10.1109/TCOMM.2022.3226190>.
 10. A. Wang, L. Lei, E. Lagunas, A. I. Prez-Neira, S. Chatzinotas, and B. Ottersten, “Joint Optimization of Beam-Hopping Design and NOMA-Assisted Transmission for Flexible Satellite Systems,” *IEEE Transactions on Wireless Communications* 21, no. 10 (2022): 8846–8858, <https://doi.org/10.1109/TWC.2022.3170435>.
 11. J. Heo, S. Sung, H. Lee, I. Hwang, and D. Hong, “MIMO Satellite Communication Systems: A Survey From the PHY Layer Perspective,” *IEEE Communications Surveys & Tutorials* 25, no. 3 (2023): 1543–1570, <https://doi.org/10.1109/COMST.2023.3294873>.
 12. Y. Liu, Y. Wang, J. Wang, L. You, W. Wang, and X. Gao, “Robust Downlink Precoding for LEO Satellite Systems With Per-Antenna Power Constraints,” *IEEE Transactions on Vehicular Technology* 71, no. 10 (2022): 10694–10711, <https://doi.org/10.1109/TVT.2022.3187046>.
 13. L. You, K.-X. Li, J. Wang, X. Gao, X.-G. Xia, and B. Ottersten, “Massive MIMO Transmission for LEO Satellite Communications,” *IEEE Journal on Selected Areas in Communications* 38, no. 8 (2020): 1851–1865, <https://doi.org/10.1109/JSAC.2020.3000803>.
 14. X. Zhang, S. Sun, M. Tao, Q. Huang, and X. Tang, “Multi-Satellite Cooperative Networks: Joint Hybrid Beamforming and User Scheduling Design,” *IEEE Transactions on Wireless Communications* 23, no. 7 (2024): 7938–7952, <https://doi.org/10.1109/TWC.2023.3346463>.
 15. Z. Xiang, X. Gao, K.-X. Li, and X.-G. Xia, “Massive MIMO Downlink Transmission for Multiple LEO Satellite Communication,” *IEEE Transactions on Communications* 72, no. 6 (2024): 3352–3364, <https://doi.org/10.1109/TCOMM.2024.3367726>.
 16. K.-X. Li, L. You, J. Wang, et al., “Downlink Transmit Design for Massive MIMO LEO Satellite Communications,” *IEEE Transactions on Communications* 70, no. 2 (2022): 1014–1028, <https://doi.org/10.1109/TCOMM.2021.3131573>.
 17. A. Abdelbadie, M. Mostafa, S. Bameri, R. H. Gohary, and D. Thomas, “DoA Estimation for Hybrid Receivers: Full Spatial Coverage and Successive Refinement,” *IEEE Transactions on Signal Processing* 2024 (2024): 1–15, <https://doi.org/10.1109/TSP.2024.3459422>.
 18. N. Khairallah and Z. M. Kassas, “Ephemeris Tracking and Error Propagation Analysis of LEO Satellites With Application to Opportunistic Navigation,” *IEEE Transactions on Aerospace and Electronic Systems* 60, no. 2 (2024): 1242–1259, <https://doi.org/10.1109/TAES.2023.3325797>.
 19. J. Pan, M. Sun, Y. Wang, and X. Zhang, “An Enhanced Spatial Smoothing Technique With ESPRIT Algorithm for Direction of Arrival Estimation in Coherent Scenarios,” *IEEE Transactions on Signal Processing* 68 (2020): 3635–3643, <https://doi.org/10.1109/TSP.2020.2994514>.
 20. J. P. Merkofer, G. Revach, N. Shlezinger, T. Routtenberg, and R. J. G. van Sloun, “DA-MUSIC: Data-Driven DoA Estimation via Deep Augmented MUSIC Algorithm,” *IEEE Transactions on Vehicular Technology* 73, no. 2 (2024): 2771–2785, <https://doi.org/10.1109/TVT.2023.3320360>.
 21. H. Son, G. Kwon, H. Park, and J. S. Park, “Signal Model and Linear Combining Design for Multi-Numerology Massive MIMO Systems,” *IEEE Transactions on Vehicular Technology* 73, no. 6 (2024): 8598–8614, <https://doi.org/10.1109/TVT.2024.3362330>.
 22. Y. Feng, W. Zhang, Y. Ge, and G. L. Stber, “Channel Time-Variation Suppression With Optimized Receive Beamforming for High-Mobility OFDM Downlink Transmissions,” *IEEE Transactions on Communications* 70, no. 2 (2022): 1183–1196, <https://doi.org/10.1109/TCOMM.2021.3126729>.
 23. X. Chen, L. Huang, H. Zhou, Q. Li, K.-B. Yu, and W. Yu, “One-Bit Digital Beamforming,” *IEEE Transactions on Aerospace and Electronic Systems* 59, no. 1 (2023): 555–567, <https://doi.org/10.1109/TAES.2022.3181257>.
 24. Y. Vasavada, A. Dhami, and J. H. Reed, “A Low-Complexity Blind Iterative Approach for Receive-Side Hybrid Beamforming,” *IEEE Transactions on Communications* 72, no. 9 (2024): 5503–5516, <https://doi.org/10.1109/TCOMM.2024.3388843>.
 25. S. Wang, Z. Li, M. He, et al., “A Joint Hybrid Precoding/Combining Scheme Based on Equivalent Channel for Massive MIMO Systems,” *IEEE Journal on Selected Areas in Communications* 40, no. 10 (2022): 2882–2893, <https://doi.org/10.1109/JSAC.2022.3196099>.
 26. F. Liu, X. Li, X. Yang, H. Shi, B. Shi, and R. Du, “Deep Learning Based Joint Hybrid Precoding and Combining Design for Mmwave MIMO Systems,” *IEEE Systems Journal* 18, no. 1 (2024): 560–567, <https://doi.org/10.1109/JSYST.2024.3357712>.
 27. X. Zhou, X. Zhang, C. Chen, et al., “Deep Reinforcement Learning Coordinated Receiver Beamforming for Millimeter-Wave Train-Ground Communications,” *IEEE Transactions on Vehicular Technology* 71, no. 5 (2022): 5156–5171, <https://doi.org/10.1109/TVT.2022.3153928>.
 28. V. Singh, G. Eappen, W. A. Martins, et al., “Diversity Combining Scheme for Time-Varying STBC NGSO Multi-Satellite Systems,” *IEEE Communications Letters* 28, no. 4 (2024): 882–886, <https://doi.org/10.1109/LCOMM.2024.3359329>.
 29. C. Ding, J.-B. Wang, Y. Chen, et al., “Satellite-Terrestrial Assisted Multi-Tier Computing Networks With MIMO Precoding and Computation Optimization,” *IEEE Transactions on Wireless Communications* 23, no. 4 (2024): 3763–3779, <https://doi.org/10.1109/TWC.2023.3311104>.
 30. 3GPP, “Study on Solutions for NR to Support Non-Terrestrial Networks (Release 16),” 38.821. 3rd Generation Partnership Project (3GPP), (2023), Version 16.2.0.
 31. 3GPP, “Study on New Radio (NR) to Support Non-Terrestrial Networks (Release 15),” 38.811. 3rd Generation Partnership Project (3GPP), (2020), Version 15.14.0.
 32. L. Wei, S. Zhao, O. F. Bourahla, et al., “End-to-End Video Saliency Detection Via a Deep Contextual Spatiotemporal Network,” *IEEE Transactions on Neural Networks and Learning Systems* 32, no. 4 (2021): 1691–1702, <https://doi.org/10.1109/TNNLS.2020.2986823>.
 33. X. Shi, Z. Chen, H. Wang, D.-Y. Yeung, W. Wong, and W. Woo, “Convolutional LSTM Network: A Machine Learning Approach for

- Precipitation Nowcasting," in *29th Annual Conference on Neural Information Processing Systems (NIPS), Montreal, CANADA, DEC 07-12, 2015*, Vol. 28 (ACM, 2015).
34. H. Han, T. Shen, Y. Chen, et al., "A ConvLSTM-Based Blind Receiver for Physical Layer Wireless Communication," *IEEE Transactions on Vehicular Technology* 73, no. 5 (2024): 7351–7356, <https://doi.org/10.1109/TVT.2023.3342169>.
35. F. Sohrabi and W. Yu, "Hybrid Digital and Analog Beamforming Design for Large-Scale Antenna Arrays," *IEEE Journal of Selected Topics in Signal Processing* 10, no. 3 (2016): 501–513, <https://doi.org/10.1109/JSTSP.2016.2520912>.
36. I. del Portillo, B. G. Cameron, and E. F. Crawley, "A Technical Comparison of Three Low Earth Orbit Satellite Constellation Systems to Provide Global Broadband," *Acta Astronautica* 159 (2019): 123–135, <https://doi.org/10.1016/j.actaastro.2019.03.040>.
37. W. Yi, W. Zhiqing, and F. Zhiyong, "Beam Training and Tracking in mmwave Communication: A Survey," *China Communications* 21, no. 6 (2024): 1–22, <https://doi.org/10.23919/JCC.ea.2021-0873.202401>.
38. 3GPP, "Study of Radio Frequency (RF) and Electromagnetic Compatibility (EMC) Requirements for Active Antenna Array System (AAS) Base Station (Release 12)," 37.840. 3rd Generation Partnership Project (3GPP), (2013), Version 12.1.0.
39. O. E. Ayach, S. Rajagopal, S. Abu-Surra, Z. Pi, and R. W. Heath, "Spatially Sparse Precoding in Millimeter Wave MIMO Systems," *IEEE Transactions on Wireless Communications* 13, no. 3 (2014): 1499–1513, <https://doi.org/10.1109/TWC.2014.011714.130846>.
40. H. Fu, S. Roy, and L. Peng, "Asymptotic Performance Analysis of MMSE Receivers in Multicell MU-MIMO Systems," *IEEE Transactions on Vehicular Technology* 70, no. 9 (2021): 9174–9189, <https://doi.org/10.1109/TVT.2021.3101554>.
41. Y. Zhang, H. An, Y. Xing, Y. Liu, and T. Zhang, "Learning Temporal and Spatial Features Jointly: A Unified Framework for Space-Time Data Prediction in Industrial IoT Networks," *IEEE Sensors Journal* 23, no. 16 (2023): 18752–18764, <https://doi.org/10.1109/JSEN.2023.3271629>.
42. G. Cui, Y. Wang, F. Li, and W. Wang, "Completion Time Optimization With Coupled Uplink-Downlink Resource Allocation for Satellite Systems," *IEEE Transactions on Aerospace and Electronic Systems* 60, no. 5 (2024): 6958–6971, <https://doi.org/10.1109/TAES.2024.3409519>.
43. X. Zhai, X. Chen, J. Xu, and D. W. Kwan Ng, "Hybrid Beamforming for Massive MIMO Over-the-Air Computation," *IEEE Transactions on Communications* 69, no. 4 (2021): 2737–2751, <https://doi.org/10.1109/TCOMM.2021.3051397>.